IEEE Access
Multidisciplinary | Rapid Review | Open Access Journal

SPECIAL SECTION ON AI-DRIVEN BIG DATA PROCESSING: THEORY, METHODOLOGY, AND APPLICATIONS

Received May 1, 2019, accepted May 19, 2019, date of publication May 23, 2019, date of current version June 3, 2019.

Digital Object Identifier 10.1109/ACCESS.2019.2918728

Learning Human-Like Trajectory Planning on Urban Two-Lane Curved Roads From Experienced Drivers

AOXUE LI, HAOBIN JIANG, JIE ZHOU, AND XINCHEN ZHOU
School of Automotive and Traffic Engineering, Jiangsu University, Zhenjiang 212013, China

Corresponding author: Aoxue Li (ujsliaoxue748@163.com)

This work was supported in part by the National Natural Science Foundation of China under Grant 51675235 and Grant 51605199, and in part by the Postgraduate Research and Practice Innovation Program of Jiangsu Province under Grant KYCX17_1812.

ABSTRACT In the coming decades, it is a universal consensus that autonomous vehicles (AVs) and human-driven vehicles will share the traffic roads. Trajectory planning of AVs has been extensively studied from the perspective of driving safety and riding comfort. However, human-like trajectory planning has rarely been studied. In this paper, we characterize and model human driving trajectories using real vehicle field test data collected on five two-way and two-lane urban curved roads with 20 experienced drivers and 3 experimental vehicles. A differential global positioning system (GPS) and an inertial navigation system (INS) are used to measure the vehicle positions and velocities in high precision. We study the trajectory characteristics of experienced drivers on curved two-lane roads, especially the relationships between the vehicle trajectories on bidirectional two lanes. Based on long short-term memory neural network (LSTM NN), we develop a data-driven trajectory model to generate human-like driving trajectories. By comparing with other three modeling methods, the LSTM NN model was validated and tested in various cases with promising performance.

INDEX TERMS Human-like trajectory planning, LSTM NN, data-driven trajectory model, two-way & two-lane curved roads, experienced drivers.

I. INTRODUCTION

At present, autonomous vehicles (AVs), intelligent vehicles, advanced driving assistant systems (ADAS), and intelligent transportation systems (ITS) are developing rapidly and have made tremendous achievements [1]. The test fields of AVs have also been upgraded from proving grounds to actual roads [2]. At this time, more and more attention has been paid to the truth that AVs and human-driven vehicles will share roads in the coming decades [3]. Faced with this fact, we need to consider the human drivers' behavior when developing autonomous driving systems [4], i.e., the driving maneuvers of AVs should be as similar as possible to human drivers, otherwise it will easily lead to traffic accidents and arouse people's disgusts and worries about AVs. Human-like driving will provide passengers with comfortable riding, and confidence that the car can drive independently [5]; moreover, human-like driving enable surrounding drivers to better understand and predict autonomous vehicle' behavior so that they can interact with it naturally [6].

In fact, researchers have gradually begun to consider the habits and characteristics of human drivers in the studies of car-following model [7], automatic parking system [8], adaptive cruise control (ACC) [9], and so on. Combining the studies of human driving behaviors, an important research hotspot is trajectory prediction and planning of AVs on curved roads. The human-like trajectory prediction and planning methods of AVs can be classified into types: model-driven approaches and data-driven approaches. Model-driven approaches represent vehicles as dynamic models (e.g. bicycle model) or kinematic models. By giving an initial state of the vehicle and sample a set of end points, candidate trajectories are generated with consideration to the vehicle kinematic, dynamic and driving maneuver constraints [10]. In the process of trajectory generation, it is also very important to detect or estimate the obstacles' statuses (e.g. positions, velocities, accelerations, moving directions) accurately and in real time. Then, candidate trajectories are evaluated by a

The associate editor coordinating the review of this manuscript and approving it for publication was Zhanyu Ma.

cost function, and the optimal one is selected for the vehicle to execute [11]. Cost functions are carefully designed by considering efficiency, comfort and safety of AVs [5]. Kalman Filter, Monte Carlo and hidden Markov models are frequently used methods to predict a vehicle's trajectory either from a known current state or from an uncertain current state [12]. Unfortunately, the afore-mentioned methods may have heavy computation load due to generating a very large number of prototype trajectories; moreover, further difficulties can arise when adapting to different roads as humanization has been ignored. Unlike model-driven approaches, data-driven approaches usually require naturalistic driving data collection and analysis. The main methods used for acquiring vehicle trajectories are global positioning system (GPS) [13], cameras [14], and LIDAR [15]. Trajectories of human-driven vehicles are collected and clustered (typical trajectory clustering methods include hidden Markov models [16], self-organizing maps [17], and neural networks [18]) to determine typical behaviors. To reflect individual driving styles, inverse reinforcement learning [19], [20], deep belief network [21] and other deep learning techniques are adopted to distill human driving patterns from different driving conditions. However, human drivers' decision making of driving maneuver in complex scene is far from being rigorously studied.

In this paper, we characterize the vehicle trajectories of experienced drivers on 5 two-way & two-lane curved roads. Twenty participants conducted the field tests with 3 experimental vehicles which are equipped with high-precision GPS/INS system. By placing virtual landmarks on the experimental roads and defining Cartesian coordinate systems, we transform the original vehicle trajectory data into lateral positions and vehicle speeds at each virtual landmark. We combine the lateral positions in the two driving directions together by defining two operations (termed as "D_{sum}" and "D_{ave}"), and their changing rules on the 5 experimental roads are studied. Finally, we establish a human-like trajectory planning model using LSTM NN. This research proposes a trajectory planning method by learning from experienced drivers aiming at human-like autonomous driving on curved roads. The contributions of this paper include the following:

1) A comprehensive field test with 20 experienced drivers is conducted on 5 curved roads with different curvatures and the extensive data are able to reflect the characterization of human driving on curved roads.
2) A novel virtual landmark method is proposed to process the trajectory data, and we find that the trajectories of experienced drivers on curves have strong similarities under 4 specified speeds.
3) With the help of LSTM NN, we develop a human-like trajectory model on curved roads. The model can generate human-like trajectories based on vehicle speed and road curvature and its performance is proven on 2 test roads.

The remainder of the paper is organized as follows. Section II outlines related studies. The experiment setup and details for driving data collection are introduced in Section III. Section IV presents the data processing and interesting findings of lateral positions. In Section V, we establish a human-like trajectory planning model on curved roads and validate as well as test its effectiveness. Finally, concluding remarks are made in Section VI.

II. RELATED WORK

Due to model predictive control (MPC) based methods have the capabilities of handling system nonlinearities and control constraints, MPC has become a well-known method to solve trajectory generation and tracking control problems [22]. Henzler *et al.* [23] proposed a novel approach to online velocity trajectory planning for manual energy efficient driving with MPC. Qian *et al.* [24] used MPC to generate reference path with consideration of user preferences and cooperative maneuver requirements. Rapidly exploring random tree (RRT) and lattice planner are two popular planning paradigms in the field of robotics. Trajectory planning of a car-like mobile robot tracking a moving target by avoiding dynamic obstacles was developed in [25] by using smoothed RRT and smoothed bidirectional RRT. Kothari *et al.* [26] presented an algorithm using RRT to generate suboptimal paths in real time. An expansion of the state lattice framework that allowed users to incorporate controller-based motion primitives and external perceptual triggers directly into the planning process was presented in [27]. Oliveira *et al.* [28] proposed an interleaved execution of path planning and path optimization combining lattice-based planning. Because of the advantages of exploring the feasible trajectories in a quick and safe way, RRT and lattice planner have been successfully applied in AVs [29].

It is noteworthy that the reasons why human drivers generate these trajectories are not considered in the afore-mentioned researches. Understanding the principles behind the human driver's handling behavior may be more conducive to the trajectory prediction and planning of the human-like AVs. As we all know, the trajectories of human drivers can be effected by numerous factors (including the driver with his psychological-physical makeup [30], vehicle speeds [31], road geometric features [32], road vegetation [33], and weather variables [34]). Sun and Das [35] found that while driving on a curved road segment, drivers tend to move closer to the centerline when driving in the outer line, and closer to the road edge when driving in the inner lane. From three experiments, Cooper *et al.* [36] found robust effects of cognitive workload on lateral position variability and eye movements play a limited role in terms of influencing lateral position variability. It was concluded in [37] that chevrons induced drivers to move closer to the edge line and away from vehicles traveling in the opposing direction. Donnell *et al.* [38] found that wide edge lines on horizontal curves make drivers shift lateral vehicle positions to the right on the tangent section during day and night. The experimental results conducted in [39] indicated that professional drivers performed more cautiously than non-professional NP drivers as the fog density increased and the standard deviation

of professional drivers' lane positions were less than (NP) drivers in S-curve driving. Based on the above findings, different kinds of human drivers' trajectory models on curved roads were proposed. Stodart and Donnell [40] investigated vehicle lateral position during nighttime conditions on 23 horizontal curves, and an ordinary least-squares(OLS) regression model was developed to predict the vehicle lateral position at the center of the curves. Through naturalistic driving data collection and treatment, Cerni and Bassani [41] proposed a local trajectory curvature model based on the curve radius and central angle. Using regression techniques, human drivers' path deviation index (PDI) model and the path trajectory ratio (PTR) model in [42] are represented by deflection angles and horizontal curve radius.

The above studies have made meaningful attempts to model the driving trajectory of human drivers on curved roads. However, these models are developed upon special position of curves that are not applicable to generate human drives' complete trajectories on the whole road segments. In most studies, when modeling vehicle trajectories, the internal relationship between the front and back of the trajectory points has been neglected. What's more, few studies have focused on the trajectory characteristics of human drivers when driving on curved two-lane roads, especially the relationships between the vehicle trajectories on bidirectional two lanes. Another thing worth noting is that the afore-mentioned trajectory modeling methods are belong to parametric techniques. Machine learning, especially deep learning, has made great progress in image recognition [43], [44], target detection [45]–[47], language identification [48], and data mining [49], [50]. With the recent advances in data-driven model [51] and machine learning [52], one prevailing non-parametric technique is the NN-based approach, due to its accurate performance and convenient model structure. What's more, the generalization ability of NN-based model is excellent.

III. FIELD TEST

To understand the characteristics of experienced drivers' driving trajectories and further develop the human-like trajectory planning model, we conduct a field test that is detailed in the following subsections.

A. PARTICIPANTS

We recruit 5 driving instructors, 5 bus drivers and 10 taxi drivers as the representatives of experienced drivers, all with driver's license of the People's Republic of China. Experienced drivers have excellent driving ability and relatively stable driving style. More importantly, compared with novice drivers' trajectories, the randomness and occasionality of experienced drivers' trajectories are smaller. The age, gender, driving experience, and annual vehicle kilometers traveled (AVKT) are presented in Table 1.

The average age of the 20 experienced drivers is about 41.7, and 4 participants are female. The average AVKT of all the participants is 4.5×10^4 km/year and the average driving experience is about 16.8 years.

TABLE 1. Details of the participants.

Number	Average age (years)	Gender (Femal/Male)	Driving experience (years)	AVKT (kilometers)
J1-J5	48.5	1/4	23.4	4.6×10^4
J6-J10	38.5	0/5	13.6	7.6×10^4
J11-J20	39.9	3/7	15.2	4.9×10^4

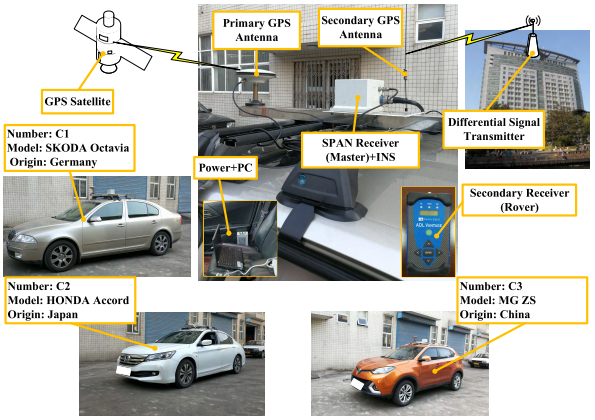

FIGURE 1. Experimental vehicles and GPS/INS.

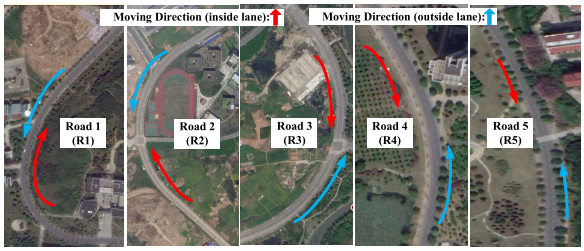

FIGURE 2. Test fields with 5 two-lane experimental roads.

B. EXPERIMENTAL VEHICLE & NAVIGATION AND POSITING SYSTEM

In this study, one SKODA Octavia, one HONDA Accord, and one MG ZS are used as the experimental vehicles, and the number of each experimental vehicle is shown in Figure 1. To record vehicle trajectories in high precision, a differential GPS system is installed on the top of experimental vehicles.

The navigation and positing system consists of a combination of GPS and INS (SDI-600GI). The acquisition accuracy can reach to $\pm$ 0.01 m when the signal is good and the sampling frequency of this system is 20 Hz. The speed, longitude, latitude, time, row, pitch as well as other data could be collected through the NovAtelConnect_1.4.0 software.

C. TEST FIELDS

The experiments are conducted on 5 two-lane roadways, with one lane in each direction. The moving directions of inside and outside lane are illustrated in Figure 2.

The actual road is not a very regular arc, but each experimental road can be assumably partitioned into three road

TABLE 2. Details of the five experimental roads.

Number	Radius of curvature (m)	Deflection angle (°)
R1	100	85.2
R2	252	94.2
R3	226	99.8
R4	140	33.6
R5	450	63.5

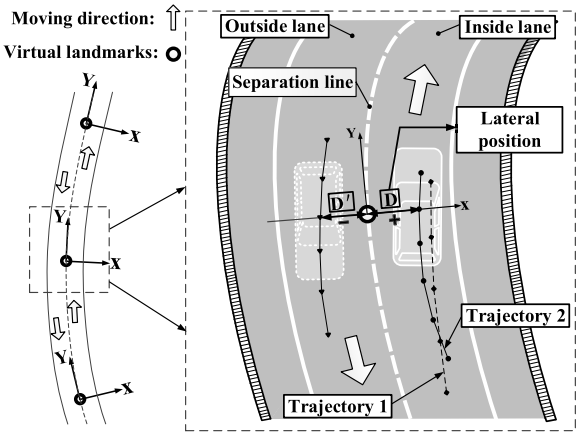

FIGURE 3. Representations of virtual landmarks and definitions of lateral positions.

segments, which are two straight line segments and one circular curve segment. The radius of curvature and deflection angle of each experimental road are illustrated in Table 2.

There were slight differences between the starting and ending points of each vehicle trajectory. Additionally, due to the differences of vehicle speeds, there is a certain degree of inconsistency between each original trajectory (e.g. trajectory 1 and trajectory 2 in Figure 3). So we place a lot of virtual landmarks along the separation line of each experimental road. The virtual landmarks are only used for calculation and they are not really set on the roads during field test. The distance between two neighboring virtual landmarks of each experimental road is equivalent and the average distance of 5 experimental roads is about 4.4 m.

Figure 3 also illustrates a partial enlarged view at the virtual landmark. Specifically, at each virtual landmark, we define a Cartesian coordinate system with Y axis being tangent to the road curve and X axis perpendicular to Y axis. Different studies have used different definitions of the lateral position. For the present study, lateral position is defined as the distance between virtual landmarks and the vehicle center of gravity. As illustrated in Figure 3, the lateral position on the inside lane D is positive, and the lateral positions on the outside lane D' is negative.

D. PROCEDURE

Each experimental road has two moving directions, experienced drivers drive on each moving direction 5 times with 4 specified vehicle speed, 20 km/h, 30 km/h, 40 km/h, and 50 km/h, respectively. Before each test, the experienced drivers are informed about the required vehicle speed for the current test and asked to keep this speed as much as possible during their driving. All participants are explicitly informed about the contents of the experiment. Since there are 3 experimental vehicles and the experimental roads are separated, the participants take turns to carry out their tests and each participant's total test time is about 7 hours. During the course of the experiment, the participants can ask for rest at any time. Throughout the experiment, perceptual blindness and drowsiness did not occur on any driver.

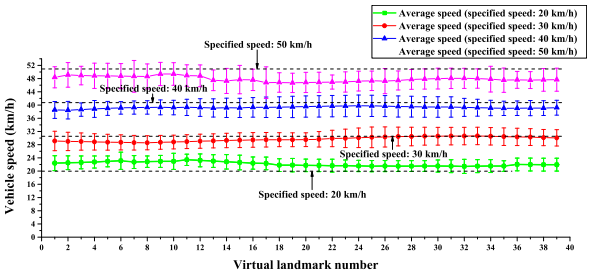

FIGURE 4. Average speed and average SD of experienced drivers on experimental road R4 (inside lane).

IV. EXPERIMENTAL RESULTS

The field test collects a total of 12000 pieces of data, among which the valid data are 11085 pieces. Each piece of data records one trajectory, and the calculation results of vehicle speeds and lateral positions are depicted in the following subsections.

A. VEHICLE SPEED

When analyzing vehicle speeds, the speed data are processed by averaging:

$$\overline{V} = \frac{1}{N \cdot T} \sum_{i=1}^{T} \sum_{j=1}^{N} v_{TN}, \tag{1}$$

where T is the number of tests at one specified speed, and N is the virtual landmark number. Meanwhile, average standard deviation (SD) is introduced to facilitate the expression:

$$\overline{SD} = \frac{1}{N} \sum_{i=1}^{N} SD_i, \tag{2}$$

where SD_i is standard deviation of all the vehicle speeds at i-th virtual landmark.

Figure 4 and Figure 5 show how experienced drivers change their speeds on experimental road R4 when driving experimental vehicle C2. The abscissas in these two figures are virtual landmark number, and the ordinates are average vehicle speed. What's more, the specified speeds are also marked by dotted lines.

As can be seen from Figure 4 and Figure 5, the average speeds of experienced drivers are close to the specified speeds, and the average SDs are not big.

Table 3 gives detailed information of vehicle speeds on 5 experimental roads. When the specified speeds are 20 km/h and 30 km/h, the average speeds of the experienced drivers are almost the same as the specified speeds; but when the

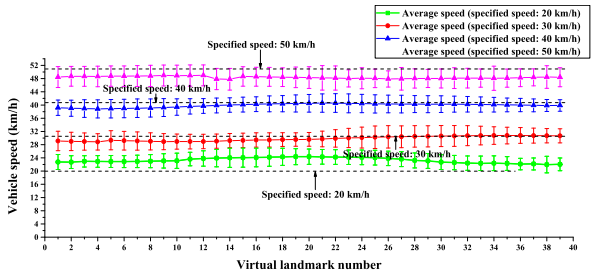

FIGURE 5. Average speed and average SD of experienced drivers on experimental road R4 (outside lane).

TABLE 3. Average speed and average SD of experienced drivers on five experimental roads.

		Specified speed: 20 km/h	Specified speed: 30 km/h	Specified speed: 40 km/h	Specified speed: 50 km/h
R1	average speed (km/h)	23.47	29.52	37.44	46.22
	average SD (km/h)	2.04	2.66	3.15	3.87
R2	average speed (km/h)	22.61	28.52	38.27	47.34
	average SD (km/h)	2.23	2.83	3.26	4.38
R3	average speed (km/h)	23.12	27.79	37.62	46.31
	average SD (km/h)	1.93	3.44	3.72	4.96
R4	average speed (km/h)	19.25	27.02	36.81	45.96
	average SD (km/h)	2.04	2.46	3.16	3.88
R5	average speed (km/h)	20.17	31.26	39.51	48.68
	average SD (km/h)	3.26	3.84	4.72	5.56

specified speeds are 40 km/h and 50 km/h, the average speeds are slightly smaller than the specified speeds. The maximum value of average SD is 5.56 and the minimum value is 1.93. It can be seen that the speed control of experienced drivers is accurate and stable, and it basically meets the experiment requirements.

B. LATERAL POSITION

In order to calculate the lateral position at each virtual landmark, the GPS sampling point closest to the virtual landmark is selected as the feature point. As an example, see Figure 6 for two sample trajectories, $\{\cdots, P_{i-1}, P_i, P_{i+1}, \ldots\}$, and $\{\ldots, Q_{j-2}, Q_{j-1}, Q_j, Q_{j+1}, Q_{j+2}, \ldots\}$.

For each virtual landmark $VL_k, k = 1, 2, \ldots, N$, we define the following neighborhood:

$$D_k := \{s | ||VL_k - s|| \leq r\}, \tag{3}$$

where r is the radius and we choose $r = 5m$ in this study. Then we searched for all GPS sampling points in the calculation domain.

Trajectory $\{\cdots, P_{i-1}, P_i, P_{i+1}, \ldots\}$ has only one GPS sampling point in the computation domain and the lateral

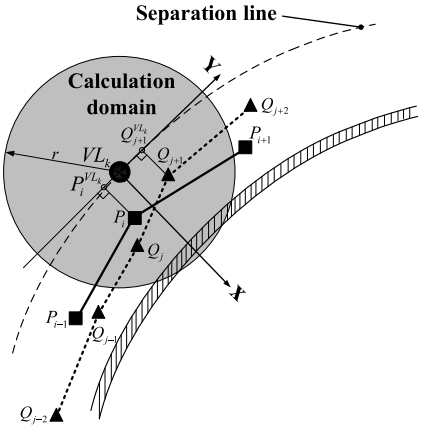

FIGURE 6. Calculations of lateral positions.

position at virtual landmark VL_k is:

$$D_k^P = \overline{P_i P_i^{VL_k}}, \tag{4}$$

where D_k^p is the lateral position at the k-th virtual landmark. The point $P_i^{VL_k}$ is obtained by perpendicular line from point P_i to the Y axis.

For trajectory $\{\cdots, Q_{j-2}, Q_{j-1}, Q_j, Q_{j+1}, Q_{j+2}, \ldots\}$, it has two sampling points in the calculation domain. Multiple sampling points may also occur during the actual calculation. When two or more sampling points appear, the linear distance between each sampling point and virtual landmark VL_k is calculated first. And it is found that:

$$\overline{Q_{j+1} VL_k} < \overline{Q_j VL_k}. \tag{5}$$

So Q_{j+1} is selected as the feature sampling point. The lateral position is:

$$D_k^Q = \overline{Q_{j+1} Q_{j+1}^{VL_k}}. \tag{6}$$

Through the above calculation, each vehicle trajectory can be expressed by a series of state variables: $\{VL_1^{t_n}, VL_2^{t_n}, \ldots, VL_k^{t_n}, \ldots, VL_N^{t_n}\}$. $VL_k^{t_n}$ contains three elements $[\rho_k, v_k^{t_n}, D_k^{t_n}]$, k is visual landmark number and t_n is the n-th test; ρ_k, $v_k^{t_n}$, and $D_k^{t_n}$ are the road curvature, vehicle speed, and lateral position of the n-th trajectory at the k-th virtual landmark.

Partial lateral positions of one experienced driver when driving experimental vehicle C1 on road R3 (both the inside and outside lanes) are illustrated in Figure 7.

It appears from Figure 7 that whether on inside or outside lane, the trends of lateral positions are similar even at different specified speeds. Horizontal comparisons of the lateral positions between the inside and outside lane show that the magnitude of the lateral positions are different, but the differences are very small. Another interesting finding is that the widths of the experiment vehicle is 1.7 m, which indicates that experienced drivers have different degrees of deviation into the opposite lane. Similar results are found in other trajectories.

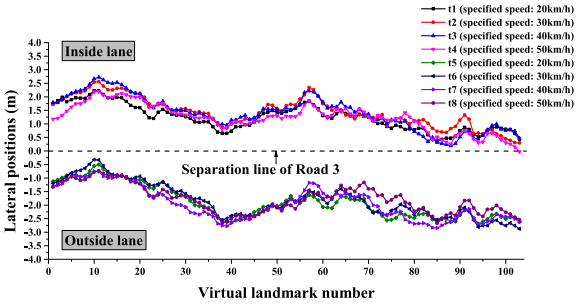

FIGURE 7. Lateral positions of one experienced driver on experimental road R3.

TABLE 4. *DTW* of experienced drivers' trajectories.

Dynamic time warping				
Specified speed	20 km/h	30 km/h	40 km/h	50 km/h
20 km/h	1.5245	1.5379	1.9976	2.3227
30 km/h	-	1.3787	1.8287	2.1297
40 km/h	-	-	1.9959	2.2919
50 km/h	-	-	-	2.4156

After collecting the trajectory data, we find that the similarities between all the drivers' trajectories are very high on each experimental road. In our paper, the vehicle trajectories are transformed into sequential data by data process. For sequential data, dynamic time warping (DTW) is an effective and simple method for calculating similarity [53], [54] and it does not require preset parameters. Before comparing two sequential data under DTW, we normalize them to have the same mean and variance. For $T = t_1, t_2, \ldots, t_i, \ldots, t_m$, the z-normalization algorithm:

$$\hat{t}_i = \frac{t_i - \mu}{\sigma}, \tag{7}$$

where μ and σ donate mean and standard deviation of T. The normalization result of T is $\hat{T} = \hat{t_1}, \hat{t_2}, \ldots, \hat{t_i}, \ldots, \hat{t_m}$.

Suppose we have two sequential data of trajectories $T = t_1, t_2, \ldots, t_i, \ldots, t_m$ and $C = c_1, c_2, \ldots, c_j, \ldots, c_n$. The DTW distance between T and C is denoted by $DTW(T, C)$:

$$DTW(T, C) = \sqrt{D(T, C)}, \tag{8}$$

$$D(T, C) = dist(t_i, c_j) + min \begin{cases} D(t_{i-1}, c_j) \\ D(t_i, c_{j-1}) \\ D(t_{i-1}, c_{j-1}) \end{cases} \tag{9}$$

where $D(t_0, c_0) = 0$, $D(t_i, c_0) = D(t_0, c_j) = \infty$, $i = 1, 2, \ldots, m$, and $j = 1, 2, \ldots, n$. Typically the Euclidean distance is used, so $dist(t_i, c_j) = (t_i - c_j)^2$. In this paper, on the same road, the lengths of T and C are the same (i.e. $m = n$).

The calculation results of all the trajectories collected on experimental road R1 are illustrated in the following table. Each value in the table is an average value of DTW.

When the specified travel speed is 30 km/h, the DTW reaches the minimum value of about 1.3787. It shows that the similarities of experienced drivers' lateral positions are high. It also indicates that experienced drivers maintain a relatively stable driving behavior during the driving on the curves.

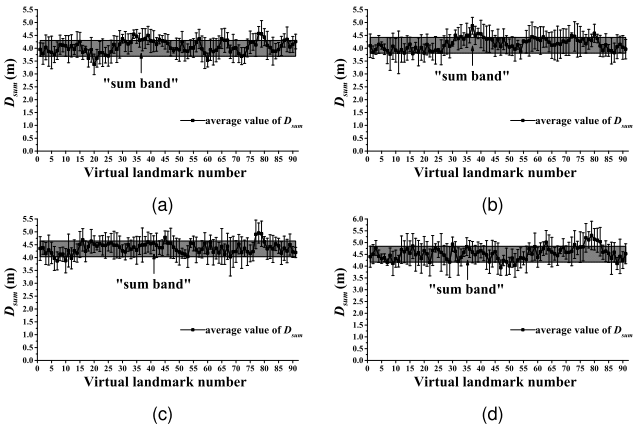

FIGURE 8. The average and SD of D_{sum} on experimental road R2. (a) Specified speed: 20 km/h. (b) Specified speed: 30 km/h. (c) Specified speed: 40 km/h. (d) Specified speed: 50 km/h.

To be more precise, the differences in the personalization of experienced drivers has little effect on their trajectories in the experimental scenario of this paper.

C. SUM AND AVERAGE OF LATERAL POSITIONS

To combine the lateral positions on the inside and outside lane together, two operations (termed as D_{sum} and D_{ave}) are introduced, and their arithmetic expressions are presented in (10) and (11):

$$D_{sum} = |D| + |D'|, \tag{10}$$

$$D_{ave} = \frac{(D + D')}{2}, \tag{11}$$

where D is the lateral position on the inside lane, and D' is the lateral position on the outside lane.

Figure 8 illustrates the calculated results of the sums of lateral positions on experimental road R2.

We include all D_{sum} in one data band (termed as "sum band"), and we find that the height of "sum band" is relative narrow. We use gray shadows to represent "sum band" in above four figures and the height of each "sum band" is 0.5 m. The average SDs of D_{sum} in Figure 8 are 0.3691 m, 0.3945 m, 0.3970 m, and 0.4433 m.

The average and SD of D_{ave} on experimental road R2 are illustrated in Figure 9.

Each curve in Figure 9 is termed as an "average line". On the whole, all "average lines" indicate very little difference in amplitude from No.1 to No.91 virtual landmark. The average SDs of D_{ave} are 0.1709 m, 0.1975 m, 0.2160 m, and 0.2334 m. From the average SDs of D_{sum} and D_{ave}, it can be seen that there are strong internal relationships between the trajectories in the two directions. There are slight differences between the width of "sum band" and the trend of "average line" in different curve driving conditions, but combined with the calculation results of DTW, it can be concluded that: The trajectories of experienced drivers on curves have very strong similarities, and the trajectories are with regularity to conform to.

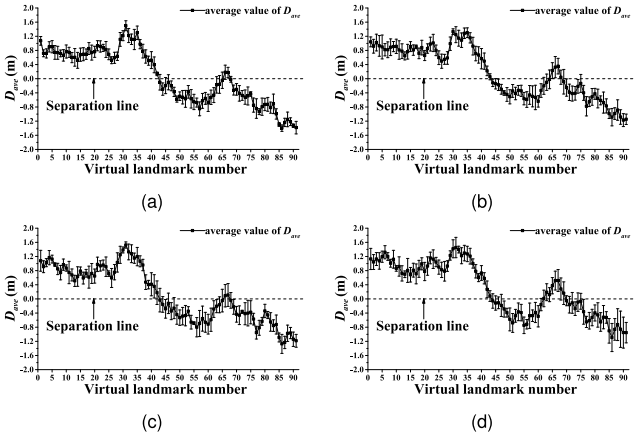

FIGURE 9. The average and SD of D_{ave} on experimental road R2. (a) Specified speed: 20 km/h. (b) Specified speed: 30 km/h. (c) Specified speed: 40 km/h. (d) Specified speed: 50 km/h.

V. MODEL ESTABLISHMENT

After converting the trajectory data that are previously difficult to unify into state variables, we obtain a lot of sequence data with the characteristics of experienced drivers' trajectories. Recurrent neural network (RNN) has unique advantages in modeling sequential data and it has the ability to memorize long-term dependencies. However, with time lags increasing, gradients of RNN may vanish through unfolding RNN into very deep feed forward neural networks. In order to overcome the disadvantages of traditional RNN, LSTM NN is proposed in this study to establish the trajectory model of experienced drivers based on field test data. LSTM NN now is wildly used in the prediction of sequence data (e.g. pedestrian trajectory prediction [55], intrusion detection [56], traffic speed prediction [57], and traffic flow prediction [58]). Although the object of our research is human drivers' trajectories on curves, based on the successful experience of aforementioned papers, we believe we can also use LSTM NN to build a human-like trajectory model with data-driven method.

A. LSTM

The typical structure of LSTM NN cells is illustrated in Figure 10. LSTM NN has a gating control mechanism that allows the network to forget past state in the memory or learn when to update its state given new information.

Let us denote the input sequence as $x = (x_1, x_1, \ldots, x_n,)$, output sequence as $y = (y_1, y_1, \ldots, y_n,)$. LSTM NN does the computation as follows:

$$i_n = \sigma(W_{xi}x_n + W_{hi}h_{n-1} + b_i), \tag{12}$$
$$f_n = \sigma(W_{xf}x_n + W_{hf}h_{n-1} + b_f), \tag{13}$$
$$o_n = \sigma(W_{xo}x_n + W_{ho}h_{n-1} + b_o), \tag{14}$$
$$g_n = \tanh(W_{xc}x_n + W_{hc}h_{n-1} + b_c), \tag{15}$$
$$c_n = f_n \odot c_{n-1} + i_n \odot g_n, \tag{16}$$
$$h_n = o_n \odot \tanh(c_n), \tag{17}$$
$$y_n = W_{hy}h_n + b_y, \tag{18}$$

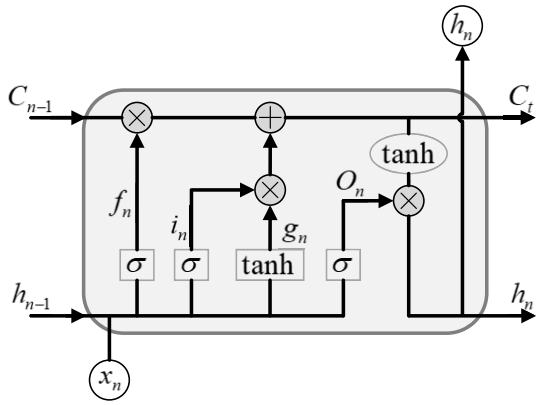

FIGURE 10. Structure of LSTM NN.

where $\odot$ represents Hadamard product, W_{xi}, W_{hi}, W_{xf}, W_{hf}, W_{xo}, W_{ho}, W_{xc}, W_{hc}, and W_{hy} are coefficient matrixes, b_i, b_f, b_o, b_c, and b_y are bias vectors, i_n is input gating vector, f_n is forget gating vector, o_n is output gating vector, g_n is state update vector, h_n is hidden state of memory cells.

$\sigma(\cdot)$ denotes the standard logistics sigmoid function defined in (19):

$$\sigma(x) = \frac{1}{1 + e^{-x}}. \tag{19}$$

$\tanh(\cdot)$ the hyperbolic tangent function:

$$\tanh(x) = \frac{e^{x} - e^{-x}}{e^{x} + e^{-x}}. \tag{20}$$

The square loss function is used as the objective function:

$$u = \frac{1}{n}\Sigma_{i=1}^{n}(y_i - p_i)^2, \tag{21}$$

where y is the real output and p is the predicted value of lateral positions.

LSTM NN is composed of 1 input layer, 2 LSTM layers with memory blocks, and 1 output layer. We design two kinds of LSTM layers, one's each hidden layer has 150 neurons (donated as $h_{150} \times h_{150}$) and the other one's each hidden layer has 300 neurons (donated as $h_{300} \times h_{300}$). There are two kinds of inputs and outputs for LSTM NN: one's inputs are $\begin{bmatrix} \rho_{k-1} & v_{k-1} \\ \rho_k & v_k \end{bmatrix}$ (ρ_{k-1} and ρ_k are road curvatures at virtual landmark $k-1$ and virtual landmark k, v_{k-1} and v_k are vehicle speeds at virtual landmark $k-1$ and virtual landmark k), the output is $[D_k]$ (lateral position at virtual landmark k), and this kind of inputs and outputs is donated as I_2O_1; the other one's inputs are $\begin{bmatrix} \rho_{k-4} & v_{k-4} \\ \rho_{k-3} & v_{k-3} \\ \rho_{k-2} & v_{k-2} \\ \rho_{k-1} & v_{k-1} \\ \rho_k & v_k \end{bmatrix}$, and the outputs are $\begin{bmatrix} D_k \\ D_{k+1} \end{bmatrix}$ (donated as I_5O_2). When modeling human drivers' trajectories with LSTM NN, we do not directly set the speed and road curvature as fixed values, the actual speeds and road curvatures in each set of state variables are used. Before training, min-max normalization is applied to scale the feature data linearly between 0 and 1. Based on back propagation through time, LSTM NN is trained by Adam optimizer. Besides, the learning rate is 0.001, and the number of epoch

TABLE 5. Hyperparameter settings.

Hyperparameter	Value
Input data	$\begin{bmatrix}\rho_{k-1} & v_{k-1}\\ \rho_k & v_k\end{bmatrix}, \begin{bmatrix}\rho_{k-4} & v_{k-4}\\ \rho_{k-3} & v_{k-3}\\ \rho_{k-2} & v_{k-2}\\ \rho_{k-1} & v_{k-1}\\ \rho_k & v_k\end{bmatrix}$
Output data	$[D_k], \begin{bmatrix}D_k\\ D_{k+1}\end{bmatrix}$
LSTM layers	2
LSTM layer neurons	(150,300)
Learning rate	0.001
Epoches	3000

is 3000. Programming language is Python 3.5 with scientific computing library ''Tensorflow'' (1.9.0) and deep learning library ''Keras'' (2.2.2). The summary of hyperparameter settings is shown in Table 5.

B. PERFORMANCE INDEX

The models' prediction performances are evaluated by mean bias error (MBE), mean absolute error (MAE), and root mean squared error (RMSE):

$$\text{MBE} = \frac{1}{n}\sum_{i=1}^{n}(\hat{y}_i - y_i), \tag{22}$$

$$\text{MAE} = \frac{1}{n}\sum_{i=1}^{n}|\hat{y}_i - y_i|, \tag{23}$$

$$\text{RMSE} = \sqrt{\frac{1}{n}\sum_{i=1}^{n}(\hat{y}_i - y_i)^2}. \tag{24}$$

MBE indicates if the observed lateral positions are overestimates or underestimated. MAE and RMSE measure residual errors, which give a global idea of the difference between the observed and predicted values.

C. RESULT AND DISCUSSION

We use 80% of the field test data for training, and the remaining 20% for validation. In order to illustrate the prediction effect of LSTM NN, three comparative models are established: autoregressive moving average model with exogenous inputs model (ARMAX) [59], back propagation neural network (BPNN) [60], and nonlinear autoregressive networks with exogenous inputs (NARX) [61].

1) PREDICTION PERFORMANCES IN VALIDATION PERIOD

For ARMAX model, one order difference is used to transform lateral positions into stationary sequence. We design two kinds of hidden layer structures of BPNN: the first kind has only one hidden layer, the number of nodes is 20, which is denoted as h_{20}; the second kind has two hidden layers, and the number of nodes are 4 and 25, which is denoted as $h_4 \times h_{25}$. The input of BPNN are $[\rho_k v_k]$ and output is $[D_k]$. The input delay orders of NARX is 2, and NARX has the same hidden layer structure as BPNN, which are denoted as h_{20} and $h_4 \times h_{25}$. The training step of BPNN and NARX is 1000 and the learning rate is 0.005. The prediction performances of the ARMAX, BPNN and NARX models are illustrated in Table 6. The algorithm with the best performance and the one with the second best performance are marked in bold and italics, respectively.

TABLE 6. Prediction performances of the ARMAX, BPNN, NARX, and LSTM NN models in validation period.

			MBE	MAE	RMSE
Inside lane	ARMAX		**-0.0163**	0.3275	0.4271
	BPNN	h_{20}	-0.2177	0.3831	0.4560
		$h_4 \times h_{25}$	-0.1911	0.3549	0.4491
	NARX	h_{20}	0.0310	0.2897	0.3773
		$h_4 \times h_{25}$	0.0959	0.2227	0.3250
	LSTM	$h_{150} \times h_{150}$	0.0220	0.1338	0.1624
	(I_2O_1)	$h_{300} \times h_{300}$	-0.0830	*0.1145*	*0.1572*
	LSTM	$h_{150} \times h_{150}$	0.0345	**0.1080**	**0.1478**
	(I_5O_2)	$h_{300} \times h_{300}$	*-0.0216*	0.1384	0.1616
Outside lane	ARMAX		0.2063	0.3194	0.4026
	BPNN	h_{20}	0.1166	0.3481	0.4422
		$h_4 \times h_{25}$	0.2268	0.3361	0.4295
	NARX	h_{20}	*-0.0143*	0.2941	0.3793
		$h_4 \times h_{25}$	0.0944	0.2273	0.2845
	LSTM	$h_{150} \times h_{150}$	0.0792	0.1308	0.1671
	(I_2O_1)	$h_{300} \times h_{300}$	-0.0331	**0.1145**	0.1572
	LSTM	$h_{150} \times h_{150}$	**0.0118**	0.1216	*0.1531*
	(I_5O_2)	$h_{300} \times h_{300}$	0.0226	*0.1153*	**0.1481**

The minimum absolute value of MBE on inside lane is 0.0163. For MAE and RMSE, the minimum values are 0.1080 and 0.1478, respectively. On outside lane, the minimum RMSE is 0.1481 and it belongs to LSTM NN. From Table 6, it is clear that LSTM NN has the best prediction performance. With the increase of the hidden layers' nodes and historical input steps, the prediction accuracy of LSTM NN is generally getting higher and higher. Higher accuracy of predictions means that the trajectories generated by LSTM model are similar to those of experienced drivers. For BPNN, with the increased number of hidden layers and nodes, the prediction effect has slightly improved. NARX has the second best performance and NARX can be regarded as an optimized version of BPNN in modeling sequence data. NARX not only establishes the non-linear relationship between inputs and outputs, but also considers the past value of outputs. LSTM NN and ARMAX also add past information of output in different ways when modeling. An interesting finding is that ARMAX's RMSE are a little smaller than BPNN's on both lanes and it indicates that the overall performance of ARMAX is a little better than BPNN. Combining the common characteristics of ARMAX and NARX, one possible reason is that there is indeed a internal relationship between the front and back of the trajectory points. BPNN model splits the relationship between the trajectory data, which makes its overall prediction performance is worse than the traditional ARMAX model.

2) PREDICTION PERFORMANCES IN TESTING PERIOD

For testing the generalization ability of lateral position model on other curved roads, data acquisition are carried out again on two test roads. The participants, experimental vehicle and equipments, experimental procedures, and data processing

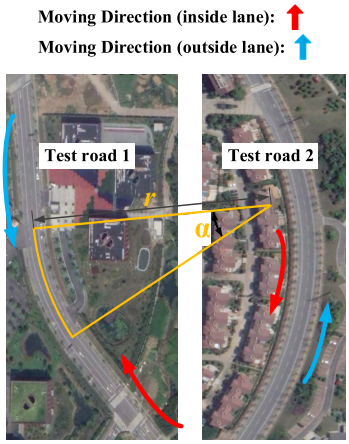

FIGURE 11. Test roads.

TABLE 7. Prediction performances of the ARMAX, BPNN, NARX, and LSTM NN models in test period.

			MBE	MAE	RMSE
Inside lane	ARMAX		0.0885	0.3269	0.4176
	BPNN	$h_4 \times h_{25}$	-0.2535	0.3770	0.4665
	NARX	$h_4 \times h_{25}$	-0.1121	0.2899	0.3821
	LSTM (I_2O_1)	$h_{300} \times h_{300}$	0.0028	0.1511	0.1921
	LSTM (I_5O_2)	$h_{300} \times h_{300}$	-0.0275	0.1462	0.1820
Outside lane	ARMAX		-0.1795	0.3423	0.4117
	BPNN	$h_4 \times h_{25}$	0.1712	0.3372	0.4535
	NARX	$h_4 \times h_{25}$	0.0723	0.3215	0.3790
	LSTM (I_2O_1)	$h_{300} \times h_{300}$	0.0804	0.1439	0.1827
	LSTM (I_5O_2)	$h_{300} \times h_{300}$	-0.0780	0.1404	0.1798

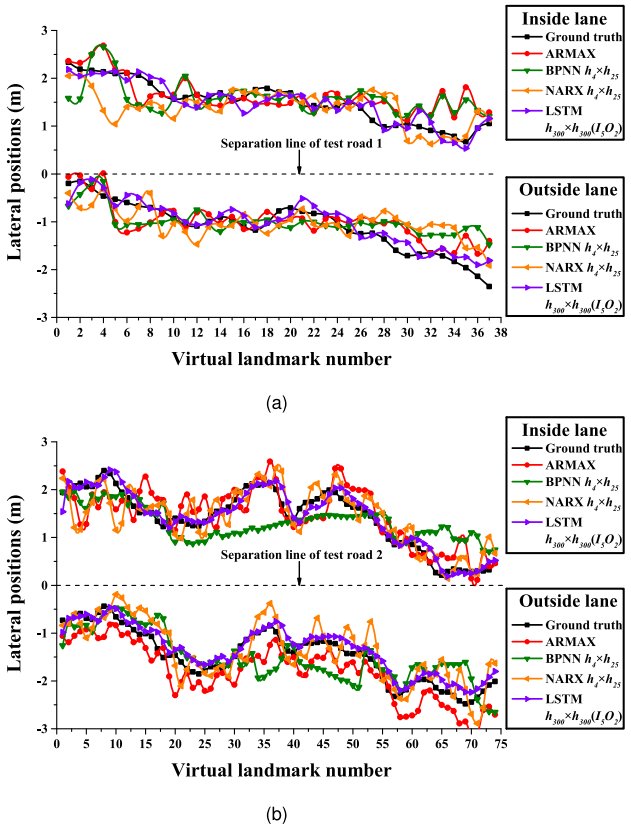

FIGURE 12. Comparison of prediction results of ARMAX, BPNN, NARX and LSTM NN (specified speed: 30 km/h). (a) Prediction results on test road 1 and (b) prediction results on test road 2.

method are the same as those described in section II and section III. As illustrated in Figure 11, the deflection angels of test road 1 and test road 2 are 27.4 ° and 48.7 ° (donated as α) and radius of curvature are 137 m and 292m (donated as r).

After selecting the valid data, the experienced drivers' trajectories on the test roads are regarded as ground truth, and ARMAX model, BPNN model, NARX model as well as LSTM NN model are used to predict the trajectories on the test roads respectively. Figure 12 (a) illustrates one piece of the prediction results of different models on test road 1 and Figure 12 (b) illustrates one piece of the prediction results of different models on test road 2.

As shown in Figure 12, the prediction results of LSTM NN are the closest to the ground truth. The results of MAE, MBE, and RMSE in Table 7 show the predicted results under 4 specified speeds on the 2 test roads.

Similar to the prediction performance in validation period, LSTM NN ($h_{300} \times h_{300}$, I_5O_2) has the best prediction performance. However, it is noted that the values of MBE, MAE and RMSE reflect that ARMAX, BPNN, NARX and LSTM NN perform slightly worse in test period than validation period. So far, the validity and generalization performance of LSTM NN-based human-like trajectory planning model have been tested.

By comparing the prediction results of different models, we find that there is an internal relationship between the front and back of the trajectory points. By virtue of the unique advantages of LSTM NN in modeling sequential data, a data-driven human-like trajectory planning model for curved roads is established. For different curved roads, continuous trajectory planning can be realized by this model. In short, given road curvatures and vehicle speeds, the obtained model can generate a trajectory that is similar to experienced human drivers, enabling human-like driving experience.

VI. CONCLUSION

In this study, we collected vehicle trajectories on 5 two-way & two-lane curved roads with 20 experienced drivers under 4 specified speeds. We processed the driving data with artificial landmarks along the separation line of each experimental road. Each piece of trajectory data was converted into state variables at each virtual landmark. To find the internal relationships between the trajectories in two driving directions, two customized formulas were introduced. From them, we found that experienced drivers follow certain boundary constraints in their driving on specific curves, and experienced drivers' trajectories on curved roads are with regularity to conform to.

Then, based on LSTM NN, we developed a human-like trajectory model by learning from experienced drivers.

The comparisons between ARMAX, BPNN, NARX and LSTM NN show that, LSTM NN has the best prediction performance in validation period. For testing the generalization performance of each model on other curved roads, data acquisition were carried out again on two test roads. The calculation results of performance index show that, the human-like trajectory planning model established in this paper can generate continuous trajectories. In reality, the trajectories of human drivers can be effected by numerous factors, and it is difficult to take all factors into account in a trajectory model. What we built using LSTM NN is a basic trajectory model. For different application scenarios, this model can add more kinds of inputs and outputs. For example, in the traffic scene of overtaking, the accelerations of ego vehicle and lead vehicle are of course very important factors, we may also need to consider time-to-collision (TTC) and so on. The obtained model can be used for free-road trajectory planning and the application scenario can be described as follows: Given the time required from the beginning to the end of the curved road, the average speed will be calculated; then a human-like trajectory under this speed can be generated according to the approach in our paper, and this trajectory will be used as the desired trajectory for trajectory tracking control.

REFERENCES

[1] K. P. Divakarla, A. Emadi, and S. Razavi, "A cognitive advanced driver assistance systems architecture for autonomous-capable electrified vehicles," *IEEE Trans. Transport. Electrific.*, vol. 5, no. 1, pp. 48–58, Mar. 2019.

[2] H. J. Vishnukumar, B. Butting, C. Müller, and E. Sax, "Machine learning and deep neural network—Artificial intelligence core for lab and real-world test and validation for ADAS and autonomous vehicles: AI for efficient and quality test and validation," in *Proc. Intell. Syst. Conf. (IntelliSys)*, Sep. 2017, pp. 714–721.

[3] E. Ohn-Bar and M. M. Trivedi, "Looking at humans in the age of self-driving and highly automated vehicles," *IEEE Trans. Intell. Veh.*, vol. 1, no. 1, pp. 90–104, Mar. 2016.

[4] K. Bengler, K. Dietmayer, B. Farber, M. Maurer, C. Stiller, and H. Winner, "Three decades of driver assistance systems: Review and future perspectives," *IEEE Intell. Transp. Syst. Mag.*, vol. 6, no. 4, pp. 6–22, Oct. 2014.

[5] X. He, D. Xu, H. Zhao, M. Moze, F. Aioun, and F. Guillemard, "A human-like trajectory planning method by learning from naturalistic driving data," in *Proc. IEEE Intell. Vehicles Symp. (IV)*, Jun. 2018, pp. 339–346.

[6] M. Zhu, X. Wang, and Y. Wang, "Human-like autonomous car-following model with deep reinforcement learning," *Transp. Res. C, Emerg. Technol.*, vol. 97, pp. 348–368, Dec. 2018.

[7] M. Lindorfer, C. F. Mecklenbräuker, and G. Ostermayer, "Modeling the imperfect driver: Incorporating human factors in a microscopic traffic model," *IEEE Trans. Intell. Transp. Syst.*, vol. 19, no. 9, pp. 2856–2870, Sep. 2018.

[8] R. Chai, A. Tsourdos, A. Savvaris, S. Chai, and Y. Xia, "Two-stage trajectory optimization for autonomous ground vehicles parking maneuver," *IEEE Trans. Ind. Informat.*, to be published.

[9] S. Moon and K. Yi, "Human driving data-based design of a vehicle adaptive cruise control algorithm," *Veh. Syst. Dyn.*, vol. 46, no. 8, pp. 661–690, 2008.

[10] L. Ma, J. Xue, K. Kawabata, J. Zhu, C. Ma, and N. Zheng, "Efficient sampling-based motion planning for on-road autonomous driving," *IEEE Trans. Intell. Transp. Syst.*, vol. 16, no. 4, pp. 1961–1976, Aug. 2015.

[11] C. Chen, Y. He, C. Bu, J. Han, and X. Zhang, "Quartic Bézier curve based trajectory generation for autonomous vehicles with curvature and velocity constraints," in *Proc. IEEE Int. Conf. Robot. Autom. (ICRA)*, May 2014, pp. 6108–6113.

[12] S. Lefèvre, D. Vasquez, and C. Laugier, "A survey on motion prediction and risk assessment for intelligent vehicles," *ROBOMECH J.*, vol. 1, no. 1, pp. 1–14, 2014.

[13] M. Imran, Y. Hassan, and D. Patterson, "GPS–GIS-based procedure for tracking vehicle path on horizontal alignments," *Comput.-Aided Civil Infrastruct. Eng.*, vol. 21, no. 5, pp. 383–394, 2006.

[14] C. Hermes, J. Einhaus, M. Hahn, C. Wöhler, and F. Kummert, "Vehicle tracking and motion prediction in complex urban scenarios," in *Proc. IEEE Intell. Vehicles Symp.*, Sep. 2010, pp. 26–33.

[15] B. Gao and B. Coifman, "Vehicle identification and GPS error detection from a LIDAR equipped probe vehicle," in *Proc. IEEE Intell. Transp. Syst. Conf.*, Sep. 2006, pp. 1537–1542.

[16] N. Saunier and T. Sayed, "Clustering vehicle trajectories with hidden Markov models application to automated traffic safety analysis," in *Proc. IEEE Int. Joint Conf. Neural Netw.*, Jul. 2006, pp. 4132–4138.

[17] W. Hu, D. Xie, T. Tan, and S. Maybank, "Learning activity patterns using fuzzy self-organizing neural network," *IEEE Trans. Syst., Man, Cybern. B, Cybern.*, vol. 34, no. 3, pp. 1618–1626, Jun. 2004.

[18] C. Hermes, C. Wohler, K. Schenk, and F. Kummert, "Long-term vehicle motion prediction," in *Proc. IEEE Intell. Vehicles Symp.*, Jun. 2009, pp. 652–657.

[19] M. Kuderer, S. Gulati, and W. Burgard, "Learning driving styles for autonomous vehicles from demonstration," in *Proc. ICRA*, May 2015, pp. 2641–2646.

[20] L. Sun, W. Zhan, and M. Tomizuka, "Probabilistic prediction of interactive driving behavior via hierarchical inverse reinforcement learning," 2018, *arXiv:1809.02926*. [Online]. Available: https://arxiv.org/abs/1809.02926

[21] D. Jeong, M. Baek, and S.-S. Lee, "Long-term prediction of vehicle trajectory based on a deep neural network," in *Proc. Int. Conf. Inf. Commun. Technol. Converg. (ICTC)*, Oct. 2017, pp. 725–727.

[22] W. Schwarting, J. Alonso-Mora, L. Paull, S. Karaman, and D. Rus, "Safe nonlinear trajectory generation for parallel autonomy with a dynamic vehicle model," *IEEE Trans. Intell. Transp. Syst.*, vol. 19, no. 9, pp. 2994–3008, Sep. 2018.

[23] M. Henzler, M. Buchholz, and K. Dietmayer, "Online velocity trajectory planning for manual energy efficient driving of heavy duty vehicles using model predictive control," in *Proc. 17th Int. Conf. Intell. Transp. Syst. (ITSC)*, Oct. 2014, pp. 1814–1819.

[24] X. Qian, I. Navarro, A. de La Fortelle, and F. Moutarde, "Motion planning for urban autonomous driving using Bézier curves and MPC," in *Proc. IEEE 19th Int. Conf. Intell. Transp. Syst. (ITSC)*, Nov. 2016, pp. 826–833.

[25] K. R. Jayasree, P. R. Jayasree, and A. Vivek, "Smoothed RRT techniques for trajectory planning," in *Proc. Int. Conf. Technol. Adv. Power Energy (TAP Energy)*, Dec. 2017, pp. 1–8.

[26] M. Kothari, D. Gu, and I. Postlethwaite, "An intelligent suboptimal path planning algorithm using rapidly-exploring random trees," in *Proc. Eur. Control Conf. (ECC)*, Aug. 2009, pp. 677–682.

[27] J. Butzke, K. Sapkota, K. Prasad, B. MacAllister, and M. Likhachev, "State lattice with controllers: Augmenting lattice-based path planning with controller-based motion primitives," in *Proc. IEEE/RSJ Int. Conf. Intell. Robots Syst.*, Sep. 2014, pp. 258–265.

[28] R. Oliveira, M. Cirillo, J. Martensson, and B. Wahlberg, "Combining lattice-based planning and path optimization in autonomous heavy duty vehicle applications," in *Proc. IEEE Intell. Vehicles Symp. (IV)*, Jun. 2018, pp. 2090–2097.

[29] D. González, J. Pérez, V. Milanés, and F. Nashashibi, "A review of motion planning techniques for automated vehicles," *IEEE Trans. Intell. Transp. Syst.*, vol. 17, no. 4, pp. 1135–1145, Apr. 2016.

[30] L. Eboli, G. Mazzulla, and G. Pungillo, "The influence of physical and emotional factors on driving style of car drivers: A survey design," *Travel Behav. Soc.*, vol. 7, pp. 43–51, Apr. 2017.

[31] C. Oh and T. Kim, "Estimation of rear-end crash potential using vehicle trajectory data," *Accident Anal. Prevention*, vol. 42, no. 6, pp. 1888–1893, Nov. 2010.

[32] S. Cafiso, A. D. Graziano, G. D. Silvestro, G. L. Cava, and B. Persaud, "Development of comprehensive accident models for two-lane rural highways using exposure, geometry, consistency and context variables," *Accident Anal. Prevention*, vol. 42, no. 4, pp. 1072–1079, 2010.

[33] A. Calvi, "Does roadside vegetation affect driving performance? Driving simulator study on the effects of trees on drivers' speed and lateral position," *Transp. Res. Rec., J. Transp. Res. Board*, vol. 2518, no. 1, pp. 1–8, 2015.

[34] A. Theofilatos and G. Yannis, "A review of the effect of traffic and weather characteristics on road safety," *Accident Anal. Prevention*, vol. 72, pp. 244–256, Nov. 2014.

[35] X. Sun and S. Das, "Safety improvement from edge lines on rural two-lane highways," Louisiana Dept. Transp. Develop., Univ. Louisiana, College Station, TX, USA, Tech. Rep. FHWA/LA.11/487, 2012.
[36] J. M. Cooper, N. Medeiros-Ward, and D. L. Strayer, "The impact of eye movements and cognitive workload on lateral position variability in driving," *Hum. Factors*, vol. 55, no. 5, pp. 1001–1014, 2013.
[37] S. T. Chrysler, J. Re, K. S. Knapp, D. S. Funkhouser, and B. T. Kuhn, "Driver response to delineation treatments on horizontal curves on two-lane roads," Texas Transp. Inst., College Station, TX, USA, 2009.
[38] E. T. Donnell, M. D. Gemar, and I. Cruzado, "Operational effects of wide edge lines applied to horizontal curves on two-lane rural highways," Texas Transp. Inst., College Station, TX, USA, Tech. Rep. FHWA/TX-09/05772-1, 2006.
[39] X. Li, X. Yan, and S. C. Wong, "Effects of fog, driver experience and gender on driving behavior on s-curved road segments," *Accident Anal. Prevention*, vol. 77, pp. 91–104, Apr. 2015.
[40] B. P. Stodart and E. T. Donnell, "Speed and lateral vehicle position models from controlled nighttime driving experiment," *J. Transp. Eng.*, vol. 134, no. 11, pp. 439–449, 2008.
[41] G. Cerni and M. Bassani, "Naturalistic driving data collection to investigate into the effects of road geometrics on track behaviour," *Transp. Res. C, Emerg. Technol.*, vol. 77, pp. 1–15, Apr. 2017.
[42] Y. J. Park, C. H. Park, and K. S. Chon, "Development of potential measures to evaluate the safety of curves in rural highways," *KSCE J. Civil Eng.*, vol. 7, pp. 233–242, May 2003.
[43] J. Han, X. Ji, X. Hu, D. Zhu, K. Li, X. Jiang, G. Cui, L. Guo, and T. Liu, "Representing and retrieving video shots in human-centric brain imaging space," *IEEE Trans. Image Process.*, vol. 22, no. 7, pp. 2723–2736, Jul. 2013.
[44] Z. Ma, Y. Lai, W. B. Kleijn, Y.-Z. Song, L. Wang, and J. Guo, "Variational Bayesian learning for Dirichlet process mixture of inverted Dirichlet distributions in non-Gaussian image feature modeling," *IEEE Trans. Neural Netw. Learn. Syst.*, vol. 30, no. 2, pp. 449–463, Feb. 2019.
[45] D. Zhang, J. Han, C. Li, J. Wang, and X. Li, "Detection of co-salient objects by looking deep and wide," *Int. J. Comput. Vis.*, vol. 120, no. 2, pp. 215–232, 2016.
[46] D. Zhang, D. Meng, and J. Han, "Co-saliency detection via a self-paced multiple-instance learning framework," *IEEE Trans. Pattern Anal. Mach. Intell.*, vol. 39, no. 5, pp. 865–878, May 2017.
[47] J. Han, D. Zhang, X. Hu, L. Guo, J. Ren, and F. Wu, "Background prior-based salient object detection via deep reconstruction residual," *IEEE Trans. Circuits Syst. Video Technol.*, vol. 25, no. 8, pp. 1309–1321, Aug. 2015.
[48] Z. Ma, H. Yu, W. Chen, and J. Guo, "Short utterance based speech language identification in intelligent vehicles with time-scale modifications and deep bottleneck features," *IEEE Trans. Veh. Technol.*, vol. 68, no. 1, pp. 121–128, Jan. 2019.
[49] G. Xiao, X. Wang, H. Luo, J. Zheng, B. Li, Y. Yan, and H. Wang, "Conceptual space based model fitting for multi-structure data," *Neurocomputing*, vol. 315, pp. 115–127, Nov. 2018.
[50] Z. Gao, R. Zhai, P. Wang, X. YanH. Qin, Y. Tang, and B. Ramesh, "Synergizing appearance and motion with low rank representation for vehicle counting and traffic flow analysis," *IEEE Trans. Intell. Transp. Syst.*, vol. 19, no. 8, pp. 2675–2685, Aug. 2018.
[51] C. Sankavaram, A. Kodali, K. R. Pattipati, and S. Singh, "Incremental classifiers for data-driven fault diagnosis applied to automotive systems," *IEEE Access*, vol. 3, pp. 407–419, 2015.
[52] X.-W. Chen and X. Lin, "Big data deep learning: Challenges and perspectives," *IEEE Access*, vol. 2, pp. 514–525, 2014.
[53] Y.-S. Jeong, M. K. Jeong, and O. A. Omitaomu, "Weighted dynamic time warping for time series classification," *Pattern Recognit.*, vol. 44, no. 9, pp. 2231–2240, Sep. 2011.
[54] J. Taylor, X. Zhou, N. M. Rouphail, and R. J. Porter, "Method for investigating intradriver heterogeneity using vehicle trajectory data: A dynamic time warping approach," *Transp. Res. B, Methodol.*, vol. 73, pp. 59–80, Mar. 2015.
[55] H. Xue, D. Q. Huynh, and M. Reynolds, "SS-LSTM: A hierarchical LSTM model for pedestrian trajectory prediction," in *Proc. IEEE Winter Conf. Appl. Comput. Vis. (WACV)*, Mar. 2018, pp. 1186–1194.
[56] C. Xu, J. Shen, X. Du, and F. Zhang, "An intrusion detection system using a deep neural network with gated recurrent units," *IEEE Access*, vol. 6, pp. 48697–48707, 2018.
[57] X. Ma, Z. Tao, Y. Wang, H. Yu, and Y. Wang, "Long short-term memory neural network for traffic speed prediction using remote microwave sensor data," *Transp. Res. C, Emerg. Technol.*, vol. 54, pp. 187–197, May 2015.
[58] Y. Tian and L. Pan, "Predicting short-term traffic flow by long short-term memory recurrent neural network," in *Proc. IEEE SmartCity*, Dec. 2015, pp. 153–158.
[59] S. D. Fassois, "MIMO LMS-ARMAX identification of vibrating structures—Part I: The method," *Mech. Syst. Signal Process.*, vol. 15, no. 4, pp. 723–735, 2001.
[60] X. Li, L. Ding, M. Shao, G. Xu, and J. Li, "A novel air-conditioning load prediction based on ARIMA and BPNN model," in *Proc. Asia–Pacific Conf. Inf. Process.*, vol. 1, Jul. 2009, pp. 51–54.
[61] J. M. P. Menezes and G. A. Barreto, "Long-term time series prediction with the NARX network: An empirical evaluation," *Neurocomputing*, vol. 71, no. 16, pp. 3335–3343, 2008.

AOXUE LI received the B.S. and M.S. degrees in vehicle engineering from Jiangsu University, Zhenjiang, China, in 2013 and 2016, respectively, where he is currently pursuing the Ph.D. degree in vehicle engineering. Since 2018, he has been a Visiting Scholar with the Department of Mechanical Engineering, Michigan State University, East Lansing, MI, USA. His research interests include autonomous vehicles, intelligent transportation systems, and ADAS technologies.

HAOBIN JIANG received the B.S. degree in agricultural mechanization from Nanjing Agricultural University, Nanjing, China, in 1991, and the M.S. and Ph.D. degrees in vehicle engineering from Jiangsu University, Zhenjiang, China, in 1994 and 2000, respectively.

From 1994 to 1995, he was a Research Assistant with the Laboratory of Power and Energy, Faculty of Biological Resources, Mie University, Mie, Japan. He joined Jiangsu University, in 1994, where he is currently a Professor of vehicle engineering. He is the Steering Technology Committee Member of the Society of Automotive Engineering of China, the Steering Technology Committee Member of the National Technical Committee of Auto Standardization, China, and the Standing Director of the Society of Automotive Engineering of Jiangsu. He is also the Dean of the School of Automotive and Traffic Engineering, Jiangsu University. His research interests include vehicle dynamic performance analysis and electrical control technology, active safety control techniques and theories of road vehicles, and intelligent transportation technology.

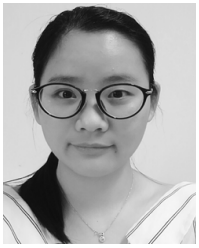

JIE ZHOU received the B.S. degree in vehicle engineering from Jiangsu University, Zhenjiang, China, in 2016, where she is currently pursuing the M.S. degree with the Department of Traffic and Transportation Engineering. Her research interests include autonomous vehicles and intelligent transportation systems.

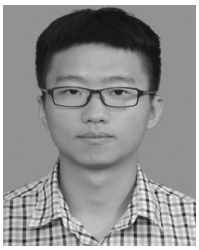

XINCHEN ZHOU received the B.S. degree in vehicle engineering from Jiangsu University, Zhenjiang, China, in 2017, where he is currently pursuing the M.S. degree with the Department of Vehicle Engineering. His research interests include automatic parking and intelligent automobiles.